



A two-pronged strategy to enhance visible-light-driven overall water splitting via visible-to-ultraviolet upconversion coupling with hydrogen-oxygen recombination inhibition



Wei Gao^{a,b}, Wenyan Zhang^{a,b,c}, Gongxuan Lu^{a,*}

^a State Key Laboratory for Oxo Synthesis and Selective Oxidation, Lanzhou Institute of Chemical Physics, Chinese Academy of Science, Lanzhou 730000, China

^b University of Chinese Academy of Science, Beijing 10080, China

^c College of Material Engineering, Jinling Institute of Technology, Nanjing, China

ARTICLE INFO

Article history:

Received 3 January 2017

Received in revised form 15 April 2017

Accepted 24 April 2017

Available online 25 April 2017

Keywords:

Visible-to-ultraviolet upconversion

Pr^{3+} - Y_2SiO_5

CaTiO_3 catalyst

Inhibition of hydrogen and oxygen recombination

Overall water splitting

Visible light irradiation

ABSTRACT

Visible-light-driven overall splitting water is a potential and sustainable approach for hydrogen generation. Although many photocatalysts have been reported to be active for this reaction, the efficiency of overall splitting water is still quite low. In this work, a two-pronged strategy is adopted to overcome two key restrictions on visible-light-driven photocatalytic overall water splitting by taking advantages of visible-to-ultraviolet upconversion (UC) effect as well as inhibiting hydrogen-oxygen recombination reaction over the photocatalyst. In order to realize that purpose, a composite photocatalyst with high stability was designed by assembling three components consisting of visible-to-ultraviolet UC Pr^{3+} - Y_2SiO_5 , UV-responsive semiconductor photocatalyst CaTiO_3 and perfluorodecalin as an oxygen transfer reagent. By the first strategy, the visible-to-ultraviolet UC unit is capable of converting visible irradiation to UV light emission, which effectively excites UV-responsive photocatalyst CaTiO_3 . The photocatalytic activity has been raised up to 200% by regulating the amount of visible-to-ultraviolet UC Pr^{3+} - Y_2SiO_5 in the designed composite photocatalyst Pr^{3+} - $\text{Y}_2\text{SiO}_5/\text{CaTiO}_3$. The photocatalyst exhibited high photochemical stability and catalytic stability in four recycle reactions. By the second strategy, hydrogen and oxygen recombination on photocatalyst surface has been effectively inhibited by an oxygen transfer reagent FDC to capture and take away newly generated oxygen from catalyst surface. This two-pronged strategy is not only convenient and efficient, but exhibits potential versatility for the most stable UV-responsive semiconductor photocatalysts to realize overall split water by visible light irradiation.

© 2017 Elsevier B.V. All rights reserved.

1. Introduction

It is urgent to explore new energy resource to replace fossil energy and severe greenhouse effects caused by over-consumption of fossil fuel [1,2]. Hydrogen is considered to be an ideal clean energy carrier to fulfill this purpose due to its high combustion enthalpy and the CO_2 zero-emission property [3–10]. Water splitting to hydrogen has been enlightened as a sustainable and highly potential approach for hydrogen production since Fujishima and Honda found that the TiO_2/Pt electrodes could facilitate water splitting, that is, generating hydrogen from pure water driven by solar energy with the aids of photocatalytic overall splitting water system [11–45].

Many efforts have been done in solar driven water splitting, however, most of the studies concentrated on the half reaction of water splitting in the presence of sacrificial reagents. For example, Cr, Ni, Cu, Nb and N codoped TiO_2 [46], CuOx/TiO_2 [47] and $\text{Ni@NiO}/\text{TiO}_2$ [48], redox-mediator-free $\text{CdS}/\text{Co}_9\text{S}_8$ hollow cubes Z-scheme photocatalyst [49], CdS nanorods with Cu_2MoS_4 as co-catalyst [50], $\text{Pt-RuS}_2/\text{Cd}_{0.5}\text{Zn}_{0.5}\text{S}$ photocatalyst [51], showed HER activity under visible light irradiation in the presence of or in the absence of sacrificial agents. And overall water splitting without sacrificial chemicals still remains challenging [52]. On the one hand, although rapid development of photocatalysts for overall water splitting has been triggered, but very seldom visible light sensitive and stable photocatalyst has been reported, for example, sulfide and selenide photocatalysts exhibit high photocatalytic activity for hydrogen evolution under visible light irradiation, but their practical applications are highly restricted due to their poor photochemical stability (photocorrosion) [53–57]. Iwashina et al. [58] used metal sulfide as hydrogen evolution photocatalyst

* Corresponding author.

E-mail address: gxlu@lzb.ac.cn (G. Lu).

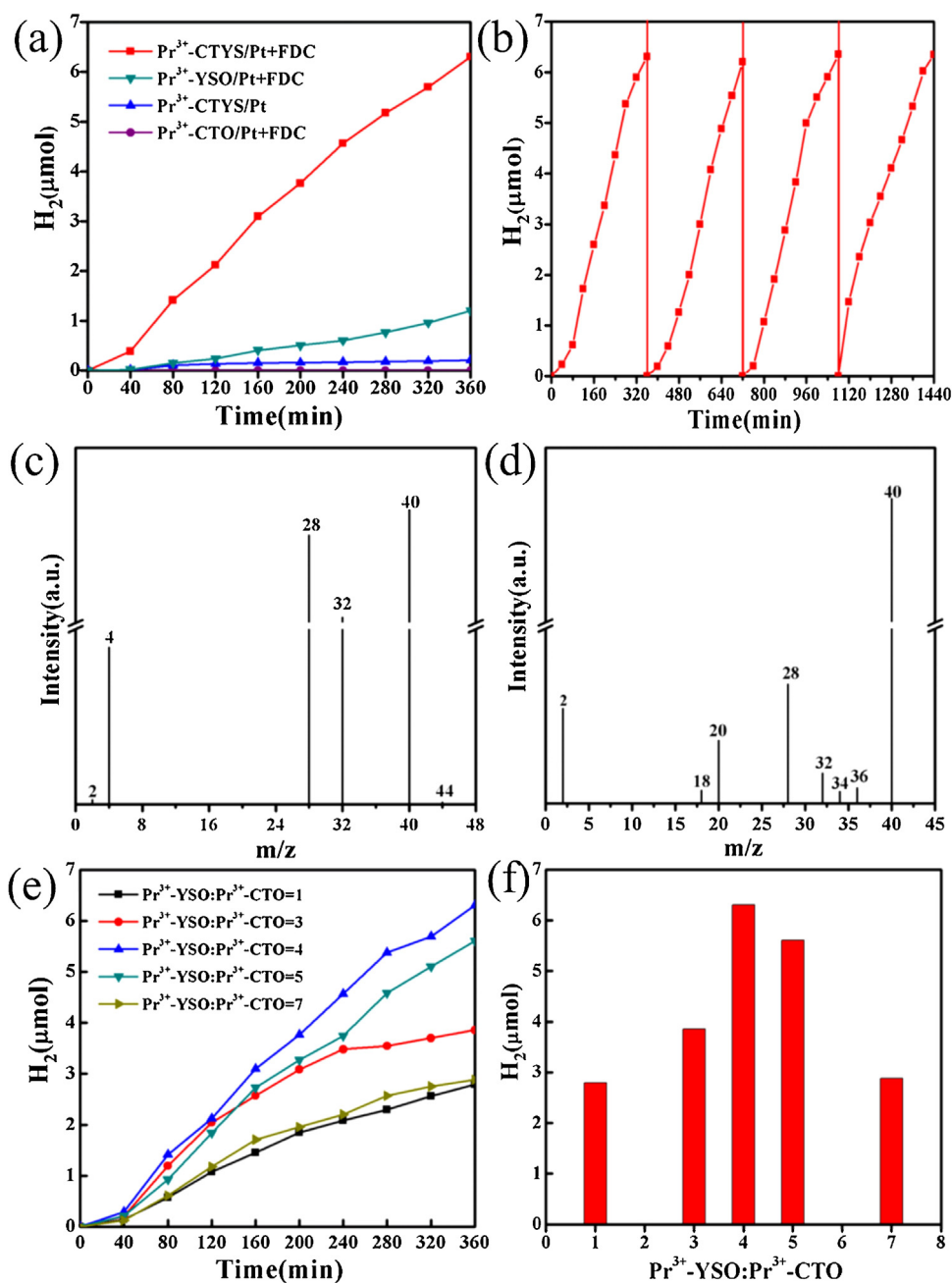
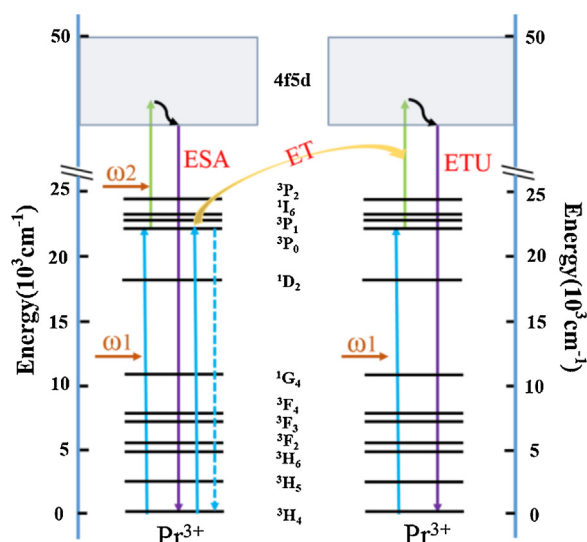


Fig. 1. (a) Photocatalytic activity of Pr³⁺-CTYS/Pt with and without FDC, Pr³⁺-CTO/Pt with FDC and Pr³⁺-YSO/Pt with FDC under visible light; (b) stability testing of Pr³⁺-CTYS/Pt; GC-MS spectra of water splitting gas products in the presence of (c) D₂O and (d) H₂¹⁸O over Pr³⁺-CTYS/Pt; (e) Photocatalytic activities and (f) maximum H₂ evolution over Pr³⁺-CTYS/Pt in the presence of FDC with the different weight ratio of Pr³⁺-YSO: Pr³⁺-CTO = 1,3,4,5,7 respectively.

accompanied with oxygen evolution photocatalyst RGO-TiO₂ in a Z-Schematic system, and they obtained stoichiometric amount of H₂ and O₂ in water splitting reaction, but the stability of their catalyst was not high enough. Zhu [59] and Wang's [60] constructed NiS/Ni foam and three-dimensional (3D) carbon paper/carbon tubes/cobalt-sulfide sheets as electrode for overall water splitting in alkaline medium, however, this photocatalyst dispersion still seems difficult for water splitting. Although some metal oxynitrides and nitrides with d⁰ transition-metal cations or typical d¹⁰ metal cations are reported to be photocatalytic under visible light irradiation for overall water splitting, such as GaN:ZnO [61], TaON [62] and Ta₃N₅ [63], but some of them are unstable under light irradiation [64], resulting from the N³⁻ ions oxidation by photogenerated holes. Carbon nitrides have been used for photocatalytic overall

water, for example, MoS₂/Co₂O₃/poly (heptazine imide) composite photocatalyst [65] can catalyze H₂ and O₂ generation using TEOA as a sacrificial hole scavenger. Pt, PtOx, and CoOx modified g-C₃N₄ [66] and Co₃O₄/Janus hollow carbon nitride spheres/Pt photocatalysts [67] were active for water splitting under UV/visible light and UV light irradiation. One difficult problem in photocatalyst development is that TiO₂ and Ti based photocatalysts are stable and active only under UV light irradiation [68–71]. One of options to overcome this obstacle is develop an upconversion (UC) material converting visible light to UV light to excite UV absorbed Ti based photocatalyst, here, the UC material could generate higher energy and shorter wavelength fluorescence under the excitation of the low energy visible photons.



Scheme 1. Visible-to-ultraviolet upconversion (UC) mechanism of Pr^{3+} in Y_2SiO_5 lattice.

Water splitting to hydrogen is also impeded by the reverse reaction of the recombination of hydrogen and oxygen molecules over the photocatalysts [72–74]. It is known that about 9.0 mg of oxygen can be dissolved in one liter of water, while only 1.63 mg of hydrogen can be dissolved in one liter of water at 20 °C and 100 kPa. Since the dissolved oxygen is about 5 times higher than that of hydrogen in water, the reverse reaction of hydrogen and oxygen recombination occurred very fast over the photocatalysts. As a result, no net hydrogen evolution could be occurred in the semiconductor dispersion. In this work, we report a “two-pronged” strategy to overcome these obstacles in visible-light-driven overall splitting water to hydrogen. A novel system was constructed by UV-responsive photocatalyst CaTiO_3 (CTO) loaded Pt NPs as a cocatalyst with high photochemical stability, visible-to-ultraviolet UC $\text{Pr}^{3+}\text{-Y}_2\text{SiO}_5$ ($\text{Pr}^{3+}\text{-YSO}$), and an oxygen transfer reagent perfluorodecalin (FDC) to capture and take newly generated oxygen away from catalyst surface. In this assembly, visible-to-ultraviolet UC unit ($\text{Pr}^{3+}\text{-YSO}$) up-converted the visible light irradiation to UV light emission for the UV-responsive photocatalyst (CTO), while hydrogen-oxygen recombination was effectively inhibited by oxygen transfer reagent (FDC). Owing to the synergistic effects of each component, the system could effectively make use of visible light irradiation and exhibit high activity and stability for visible-light-driven overall splitting water.

2. Experiments

2.1. Preparation of the photo-catalysts

The CaTiO_3 was synthesized via sol-gel method. Details are as follows, 5 mL tetrabutyl titanate (AR) was firstly mixed with 15 mL anhydrous ethanol and the obtained mixture was ultrasonic treated for 30 min, which was named solution A. The corresponding stoichiometric calcium nitrate tetrahydrate (AR) and praseodymium nitrate hexahydrate (AR) were dissolved in 7 mL anhydrous ethanol containing 1 mL distilled water while keeping the molar ratio of Ca:Ti constant 1:1, Pr^{3+} :Ti was 0.002:1 with 0.6 g boric acid as co-solvent, then the mixture was ultrasonic treated until it was completely dissolved to homogeneous solution, which was named solution B. Slowly added solution B to A under stirring, then one or two drops of concentrated HCl were added. The sol was formed quickly after addition solution B to A, then the mixture was kept at room temperature for 90 min under stirring, and dried at 80 °C

overnight, the obtained powders were calcinated at 1300 °C for 4 h, the white color powders which could emit red light under UV light irradiation were finally gained. $\text{Pr}^{3+}\text{-YSO}$ was synthesized by the similar sol-gel method as described above with ethyl or thosilicate (TEOS) as silicon source.

2.2. Preparation of the $\text{Pr}^{3+}\text{-Y}_2\text{SiO}_5$ and $\text{Pr}^{3+}\text{-Y}_2\text{SiO}_5/\text{Pr}^{3+}\text{-CaTiO}_3$ composite photocatalyst

The similar preparation method was used in $\text{Pr}^{3+}\text{-Y}_2\text{SiO}_5$ and $\text{Pr}^{3+}\text{-Y}_2\text{SiO}_5/\text{Pr}^{3+}\text{-CaTiO}_3$ ($\text{Pr}^{3+}\text{-CTYS}$) composite photocatalyst preparation, here, yttrium nitrate hexahydrate, praseodymium nitrate hexahydrate (the percentage of Pr^{3+} was 0.7 mol% to Si), boric acid, anhydrous ethanol and distilled water were mixed together and were ultrasonic treated until the mixture was completely dissolved. Then the different amount of prepared $\text{Pr}^{3+}\text{-CTO}$ were added to the mixture solution to synthesize $\text{Pr}^{3+}\text{-CTYS}$ photocatalysts, the weight ratios of $\text{Pr}^{3+}\text{-YSO}$ and $\text{Pr}^{3+}\text{-CTO}$ were finally controlled as 1:1, 3:1, 4:1, 5:1 and 7:1, respectively. The mixture was then stirred at 80 °C in a water bath while about 2 mL ammonia was added at the beginning to accelerate the process of sol formation. Finally, the sol was calcined at 1000 °C for 4 h. The $\text{Pr}^{3+}\text{-YSO}$ were prepared by the similar method without adding $\text{Pr}^{3+}\text{-CTO}$.

2.3. Photocatalytic H_2 evolution activity

Photocatalytic reactions were carried out in a sealed pyrex flask (190 mL), which has a flat window with the irradiation area about 14 cm² at room temperature. In a typical reaction, 100 mg $\text{Pr}^{3+}\text{-CTYS}$, 100 μL methanol and 250 μL 5 mg/mL K_2PtCl_6 were dispersed into 140 mL distilled water in a sealed pyrex flask to load Pt photoreduction taking place. The mixture was ultrasonic treated 30 min before bubbling Ar gas to degas for 30 min, subsequently the reactor was irradiated under UV light to load Pt on $\text{Pr}^{3+}\text{-CTYS}$. During the reduction process, the gas composition and content in the sealed Pyrex flask were monitored by gas chromatography. After photoreduction of Pt was accomplished, the mixture was continuously irradiated under UV light to completely consume methanol inside till no hydrogen could be detected. Subsequently, the catalyst itself with loaded Pt was washed with pure water, and ready for the water splitting experiment. The degassed mixture was bubbled with high pure Ar gas for 30 min again, then 1 mL of FDC was added to work as an oxygen transfer reagent to inhibit newly formed hydrogen and oxygen recombination. The photocatalyst activity of hydrogen evolution was measured under visible light using gas chromatography (Aglient 6820, TCD, 13 \times column, Ar carrier). The light source was a 300-W Xenon lamp with a 420 nm cutoff filter.

2.4. Isotopes tracer experiment

In order to demonstrate that $\text{Pr}^{3+}\text{-CTYS}/\text{Pt}$ can act as photocatalyst for overall water splitting to hydrogen and oxygen simultaneously, isotopes tracer experiments were carried out. Experimental steps were followed by the method described above, except the distilled water was changed to D_2O or H_2^{18}O for the detection of D_2 and $^{18}\text{O}_2$. The formed D_2 and $^{18}\text{O}_2$ were measured by GC-MS (MAT 271).

2.5. Photoelectrochemical measurements

All the photoelectrochemical measurements were carried out on an electrochemical analyzer (CHI660E) in a homemade standard three-electrode cell, consisting of an organic glass enclosure with a quartz window and a 1.2 cm diameter opening opposite the window to the work electrode clamped. The working electrodes were prepared by dropping the catalyst sample directly onto the surface

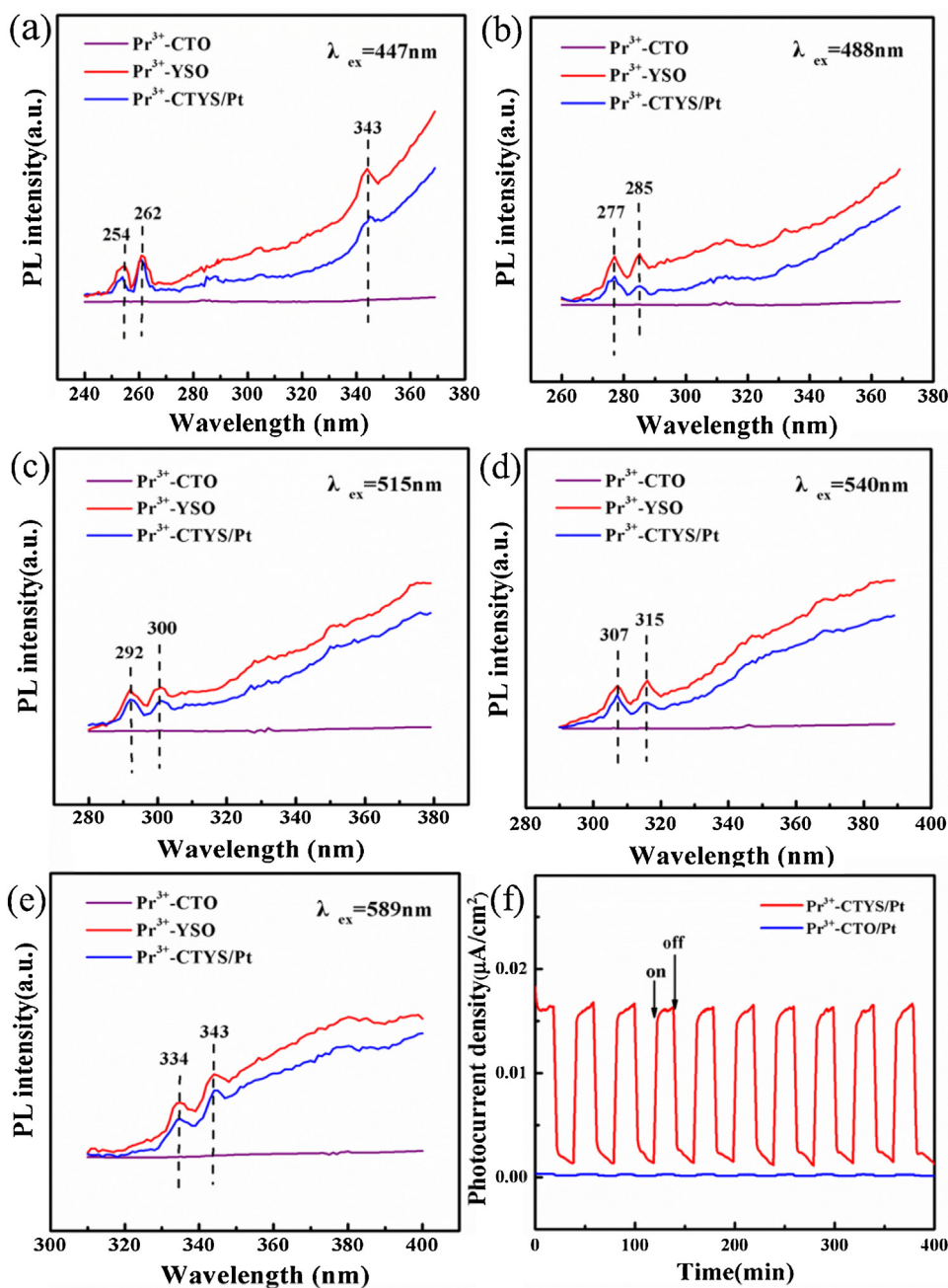


Fig. 2. (a–e) The photoluminescence (PL) spectra of the Pr³⁺-YSO, Pr³⁺-CTO and Pr³⁺-CTYS/Pt under different excitation wavelength; (f) Transient photocurrent–time curves of Pr³⁺-CTO/Pt and Pr³⁺-CTYS/Pt under visible light irradiation.

of the precleaned indium tin oxide glass (ITO glass). The area of the working electrode exposed to the electrolyte was about 1 cm². Platinum foil was used as counter electrode and a saturated calomel electrode (SCE) as the reference electrode. The current–time curve was obtained under unbiased condition to investigate the anodic photocurrent. The linear sweep voltammetry (LSV) curves were recorded with the scan rate of 1 mV s^{−1}. The excitation source was a 300-W Xenon lamp with a 420 nm cutoff filter.

The apparent quantum efficiency (AQE) was measured under the similar reaction conditions under irradiation light through a bandpass filter (417 nm). Photon flux of the incident light was determined using a Ray virtual radiation actinometer (FU 100, silicon ray detector, light spectrum, 400–700 nm; sensitivity, 10–50 μV μm mol^{−1} m^{−2} s^{−1}). The reaction solutions were irradi-

ated for 60 min with bandpass filters for AQE tests. The following equation was used to calculate the AQE.

$$\text{AQE} = \frac{2 \times \text{the number of hydrogen molecules evolved}}{\text{the number of incident photons}} \times 100\%$$

2.6. Characterizations of the catalysts

The X-ray photoelectron spectroscopy (XPS) analysis was conducted with a VG Scientific ESCALAB210-XPS photoelectron spectrometer with an Al Kα X-ray resource. X-ray diffraction patterns (XRD) of the samples were recorded on a Rigaku B/Max-RB X-ray diffractometer with a nickel-filtered Cu Kα radiation, specifically using a position sensitive detector at the step time of 15 s at 40 mA and 40 kV, scan step 0.017°, and the 2θ range was 5–90°.

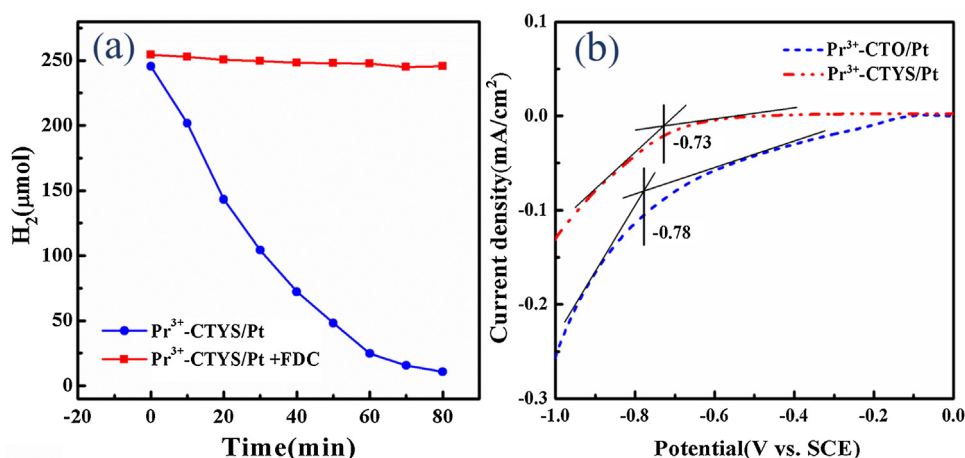
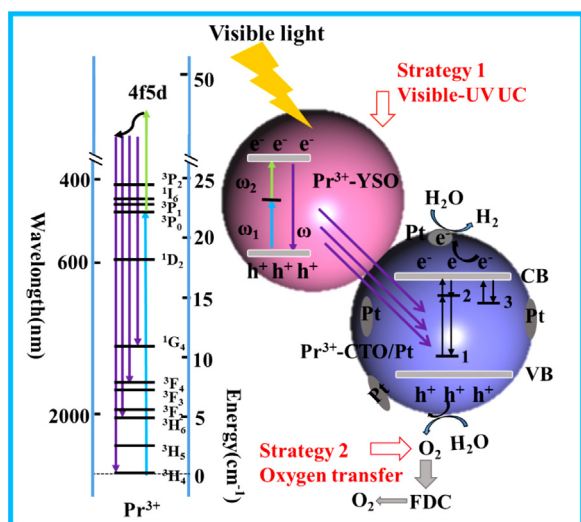


Fig. 3. (a) hydrogen recombination reaction curves over Pt^{3+} -CTYS/Pt with and without FDC; (b) LSV curves of CTO/Pt and Pt^{3+} -CTYS/Pt photocatalysts on ITO glass. (For interpretation of the references to colour in the text, the reader is referred to the web version of this article.)



Scheme 2. Two-pronged strategy of Pr^{3+} -CTYS/Pt for visible-light-driven overall water splitting.

Transmission electron microscopy (TEM) and HRTEM images were obtained using a Tecnai-G2-F30 field emission transmission electron microscope operating at accelerating voltage of 300 kV. The fluorescence spectra were measured using a Hitachi F-4500 fluorescence spectrometer with excitation wavelength at 447 nm, 488 nm, 515 nm, 540 nm and 589 nm respectively.

3. Results and discussion

Due to its wide band gap, only UV irradiation could be used by Pr^{3+} -CTO/Pt to catalyze overall water splitting. No hydrogen was detected under visible light irradiation over Pr^{3+} -CTO/Pt itself (Fig. S1). When Pr^{3+} -CTO/Pt was assembled with Pr^{3+} -YSO, the hydrogen generated in Pr^{3+} -CTYS/Pt dispersion was $6.31 \mu\text{mol g}^{-1}$ in 6 h under visible light irradiation in the presence of FDC, which was 30 times greater than that of Pr^{3+} -CTYS/Pt without FDC ($0.21 \mu\text{mol g}^{-1}$ in 6 h). It's worth noting that the single Pr^{3+} -YSO/Pt also presented the activity of hydrogen generation but was much lower than Pr^{3+} -CTYS/Pt, indicating that the activity was mainly derived from the interaction of Pr^{3+} -CTO/Pt and Pr^{3+} -YSO. The hydrogen evolution rate of Pr^{3+} -CTYS/Pt system was obviously increased in the presence of FDC. After the reaction, the combined oxygen in FDC was measured, and calculated H_2 and O_2 was about 1.2:1. This

Pr³⁺-CTYS/Pt catalyst exhibited stable recycle activity for visible-light-driven HER, and no obvious deactivation was observed after 1440 min reaction (Fig. 1(b)), indicating that assembling of Pr³⁺-YSO not only widened the working spectra response region of Pr³⁺-CTO photocatalyst to visible light, but enhanced the catalyst stability during reaction.

Isotopes tracer tests were conducted to confirm whether the $\text{Pr}^{3+}\text{-CTYS/Pt}$ could promote visible-light-driven overall water splitting. As shown in Fig. 1(c), D_2 was detected when D_2O was used in isotopes tracer test, thus proving that the H_2 were generated by photocatalytic water splitting. Meanwhile, $^{18}\text{O}_2$, $^{16}\text{O}^{18}\text{O}$ and $^{16}\text{O}_2$ were generated when H_2^{18}O was applied in isotopes tracer test, confirming that OER was promoted simultaneously with HER by splitting water. Those isotopes tracer tests identify that the $\text{Pr}^{3+}\text{-CTYS/Pt}$ is capable of overall splitting water reaction triggered by visible light irradiation.

The visible-to-ultraviolet UC capability of Pr^{3+} -YSO is attributed to the excited state absorption (ESA) and energy transfer UC (ETU) process of Pr^{3+} ions in Y_2SiO_5 lattices, as illustrated in [Scheme 1](#). In terms of the ESA, a single Pr^{3+} ion was pumped to its excited intermediate state after successively absorbing the energy of two photons (ω_1 and ω_2), and UC fluorescence was released when the excited electron transferred back to the ground state via radiation relaxation. The $^3\text{P}_j$, $^1\text{I}_6$ levels of Pr^{3+} ion can be used as intermediate excited states to achieve the ESA process, like the process of $^3\text{H}_4 \rightarrow ^3\text{P}_0 \rightarrow 4\text{f}5\text{d}$ [75–78]. In the case of ETU process, the energy transfer occurred between two neighboring Pr^{3+} ions (one as the sensitizer and the other as the activator) rather than consecutive absorption of two photons in a single Pr^{3+} ion [79]. Specifically, two Pr^{3+} ions at $^3\text{P}_0$ state interact with each other and both of them have absorbed the energy of a photon (ω_1), one Pr^{3+} transfers its energy to the another one by energy transfer (ET) process, so one Pr^{3+} goes back to the $^3\text{H}_4$ ground state, while the another one is excited into the $4\text{f}5\text{d}$ band for visible-to-ultraviolet UC. Our experiments confirmed this scheme. The capability of Pr^{3+} -CTYS/Pt for visible-light-driven water splitting is accomplished by the visible-to-ultraviolet UC ability of Pr^{3+} -YSO. As shown in [Fig. 2\(a–e\)](#), the prepared Pr^{3+} -YSO and Pr^{3+} -CTYS/Pt effectively transfer the visible light of 447 nm, 488 nm, 515 nm, 540 nm and 589 nm to 254–343 nm UV emission, which can be utilized by Pr^{3+} -CTO/Pt for overall water splitting.

The visible-to-ultraviolet UC of Pr³⁺-YSO was also investigated by transient photocurrent test. As shown in Fig. 2(f), Pr³⁺-CTO/Pt exhibited no photo-current under visible light irradiation. When the Pr³⁺-CTO/Pt was assembled with Pr³⁺-YSO,

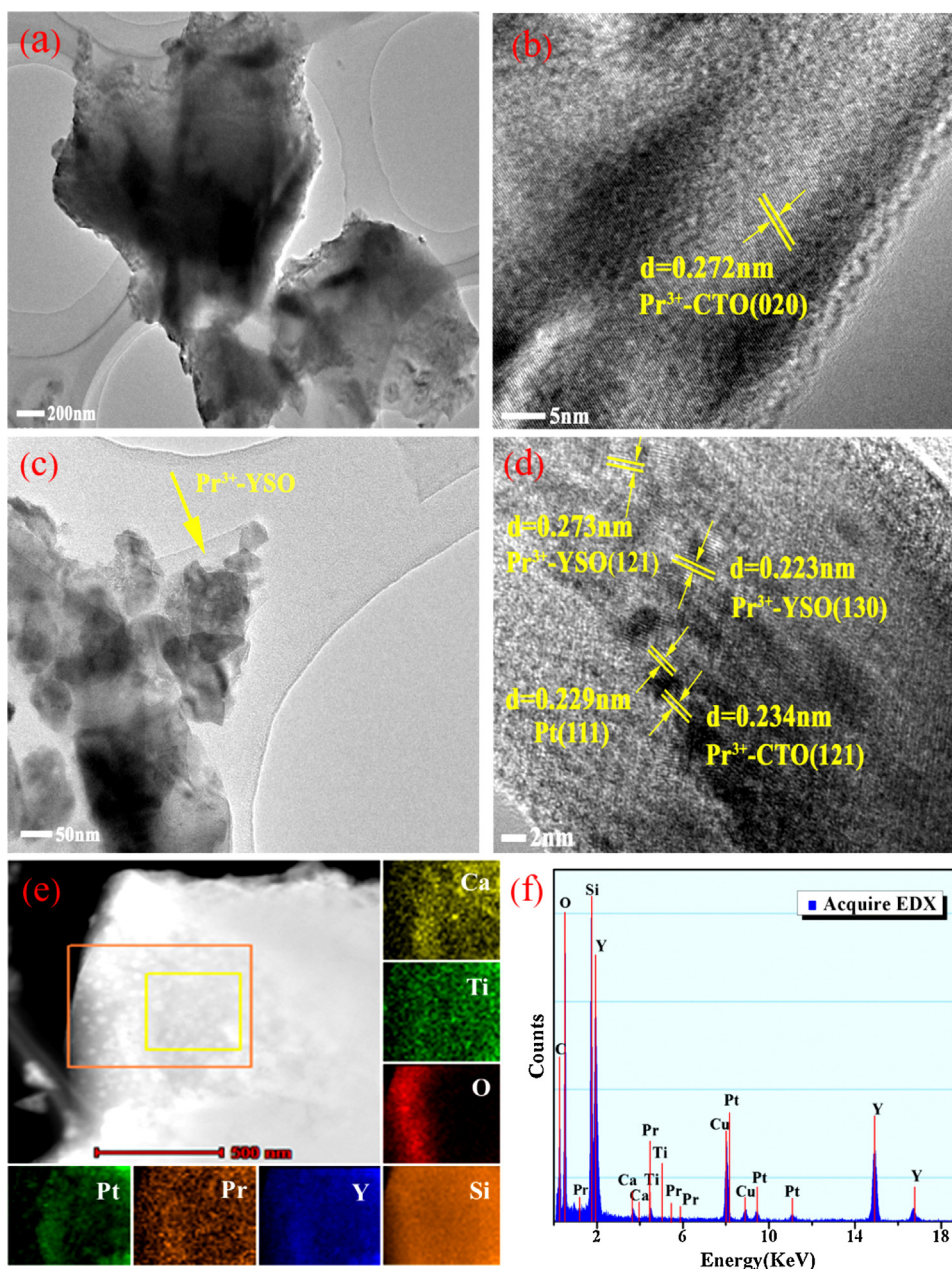


Fig. 4. (a) TEM and (b) HRTEM images of Pr^{3+} -CTO; (c) TEM and (d) HRTEM images of Pr^{3+} -CTYS/Pt; (e) Element mapping images and (f) EDX spectrum of Pr^{3+} -CTYS/Pt (the results of (e) and (f) were obtained from the region of orange rectangle). (For interpretation of the references to colour in this figure legend, the reader is referred to the web version of this article.)

Pr^{3+} -CTYS/Pt exhibited obviously enlarged photocurrent under visible light irradiation, which confirmed that incident visible light was converted to UV light by Pr^{3+} -YSO to yield large amounts of photogenerated electrons and holes in Pr^{3+} -CTO. Those photogenerated carriers then facilitate the HER and OER simultaneously over Pr^{3+} -CTO/Pt. Furthermore, in order to reveal more about the important role of Pr^{3+} -YSO in visible-light-driven water splitting, we regulated the proportion of Pr^{3+} -YSO and Pr^{3+} -CTO in the Pr^{3+} -CTYS/Pt photo-catalysts and measured their photocatalytic activities. Photocatalytic activity of the Pr^{3+} -CTYS/Pt was raised up to 200% by improving the proportion of Pr^{3+} -YSO and Pr^{3+} -CTO, as shown in Fig. 1(e, f), here, the ratio of Pr^{3+} -YSO and Pr^{3+} -CTO was 4:1. This result clearly proves the key role of Pr^{3+} -YSO in promoting water splitting driven by visible light.

According to above results, the first strategy to promote visible-light-driven overall splitting water could be illustrated in Scheme 2 as “strategy 1”, which effectively realized visible-light driven water splitting by taking advantages of an energy transfer process via the Visible-to-ultraviolet upconversion. That strategy offered a way to use visible light just assembling a UV-responsive photocatalyst with a visible-to-ultraviolet UC unit with a stable photocatalyst such as TiO_2 . “strategy 1” is not only convenient and effective, but has favorable versatility for most UV-responsive photocatalysts to realize overall split water by visible light irradiation.

Generally, about 9.0 mg of oxygen can be dissolved in one liter of water, while only 1.63 mg of hydrogen can be dissolved in one liter of water at 20 °C and 100 kPa. The concentration of dissolved oxygen is about 5 times higher than that of hydrogen in water, the recombination reaction of hydrogen and oxygen might be kinetically promoted over the photocatalysts [72–74]. We identified

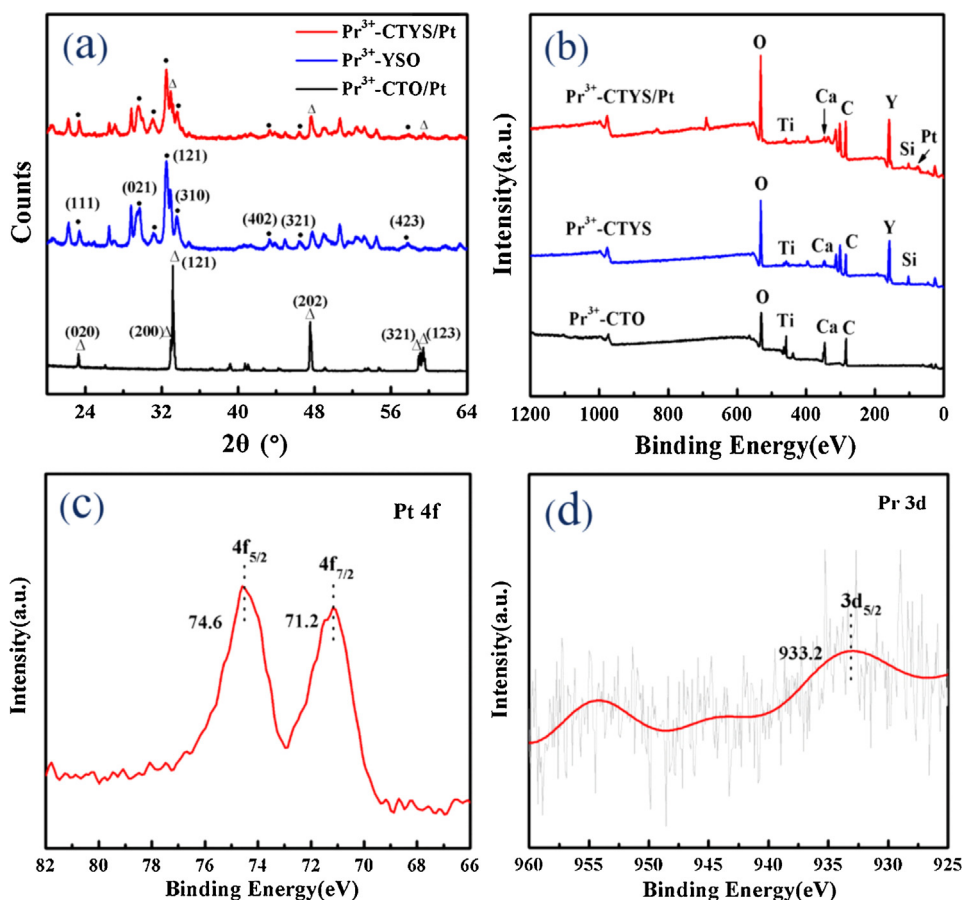


Fig. 5. (a) XRD patterns of Pr³⁺-CTO/Pt, Pr³⁺-CTYS and Pr³⁺-CTYS/Pt and (b) XPS survey of Pr³⁺-CTO, Pr³⁺-CTYS and Pr³⁺-CTYS/Pt; (c) Pt 4f XPS of Pr³⁺-CTYS/Pt (d) Pr 3d XPS of Pr³⁺-CTYS/Pt.

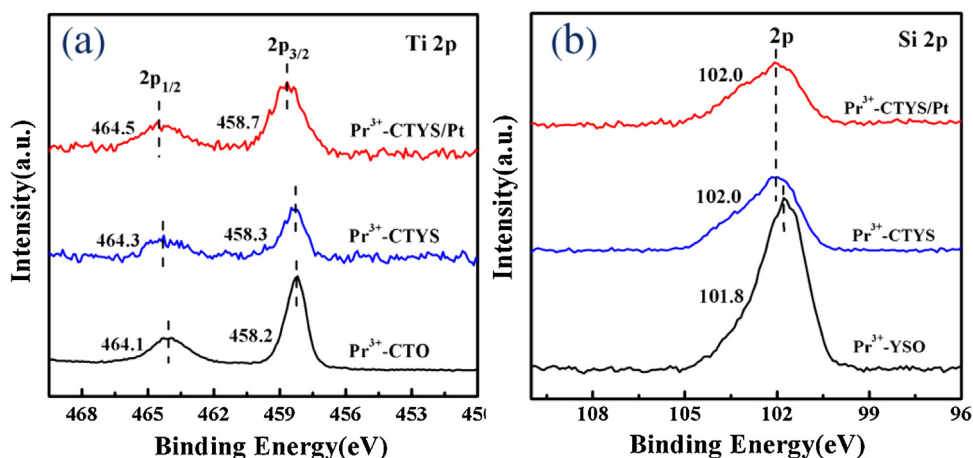


Fig. 6. (a) Ti 2p XPS spectra Pr³⁺-CTO, Pr³⁺-CTYS and Pr³⁺-CTYS/Pt and (b) Si 2p XPS spectra of Pr³⁺-YSO, Pr³⁺-CTYS and Pr³⁺-CTYS/Pt.

that similar reaction also occurred in our Pr³⁺-CTYS/Pt dispersion (Fig. 3(a), blue curve). Before the reaction, the desired amount of hydrogen was injected into the reaction. The concentration of hydrogen in the reactor decrease very significantly in the absence of oxygen transfer reagent FDC. That means the newly formed hydrogen would react with dissolved oxygen in water or photocatalytic formed oxygen to H₂O again over catalyst surface if the hydrogen and oxygen recombination process could not be inhibited. In this case, no hydrogen could be detected under irradiation. Besides, LSV tests shows that the Pr³⁺-CTYS/Pt photocatalysts exhibit lower

hydrogen evolution potential than Pr³⁺-CTO/Pt (Fig. 3(b)), indicating that hydrogen are more liable to be generated from over Pr³⁺-CTYS/Pt catalyst. That will lead to more serious hydrogen and oxygen recombination at the same time over this composite photocatalyst. Without doubt, the recombination of hydrogen and oxygen is another key obstacle in improving the efficiency of photocatalytic overall water splitting, and is necessary to be inhibited. To fulfill that purpose, strategy 2 was used simultaneously with strategy 1, as illustrated in Scheme 2. Strategy 2 was achieved by preventing the reverse reaction via transferring the photogener-

ated oxygen molecules away from the photocatalysts. Herein, FDC was selected as an oxygen transfer reagent to capture the photo-generated oxygen, because FDC not only has strong affinity and high solubility for oxygen molecules but possess excellent structural and chemical stability to resist photodecomposition [80]. Our experiments confirmed that the adding of FDC could effectively prevent the hydrogen and oxygen from recombination, as shown by the red curve in Fig. 3(a). Thereafter, the HER and OER were effectively promoted over the Pr^{3+} -CTYS/Pt photocatalyst and visible-light-driven overall splitting water were achieved.

More detailed investigation was conducted to reveal more intrinsic relationship between the structure of Pr^{3+} -CTYS/Pt photocatalyst and its high efficiency for visible-light-driven water splitting. As show in Fig. 4(a, c), Pr^{3+} -CTYS/Pt was composed of three components: Pr^{3+} -YSO, Pr^{3+} -CTO and the Pt nanoparticles (NPs). In consistent with TEM results, XRD patterns also show that the typical peaks of Y_2SiO_5 (JCPDS# 52-1810) [81] and CaTiO_3 (JCPDS# 42-0423) [82] in Pr^{3+} -CTYS/Pt photocatalyst (Fig. 5(a)). The XPS spectra were obtained to study the chemical composition and oxidation state on the Pr^{3+} -YSO, Pr^{3+} -CTO, Pr^{3+} -CTYS and Pr^{3+} -CTYS/Pt, and the interaction of Pr^{3+} -YSO and Pr^{3+} -CTO. The Y, Si, Ca, Ti and Pt elements on the surface of Pr^{3+} -CTYS/Pt originate from the Pr^{3+} -YSO, Pr^{3+} -CTO and Pt NPs, respectively (Figs. 4 (f), 5 (b)). The Pr 3d XPS shows that the Pr element mainly exist as Pr^{3+} chemical states, which could yield the visible-to-ultraviolet UC in Y_2SiO_5 lattices (Fig. 5(d)).

In addition, in Pr^{3+} -CTYS/Pt, the Pr^{3+} -YSO contact closely with Pr^{3+} -CTO to form Pr^{3+} -CTYS heterojunction (Fig. 4(d)). Ti 2p XPS and Si 2p XPS spectra confirm the formation of Pr^{3+} -CTYS heterojunction (Fig. 6). After assembling Pr^{3+} -CTO with Pr^{3+} -YSO, the Ti 2p_{3/2} binding energies blue shift from 458.2 eV to 458.3 eV, the Ti 2p_{1/2} binding energies shift from 464.1 eV to 464.3 eV, and the Si 2p binding energies shift higher to 102.0 eV. Those blue shifts of Ti and Si binding energy indicate the strong interaction and overlapping electron cloud were generated on the heterojunction between Pr^{3+} -CTO and Pr^{3+} -YSO. Moreover, as Pr, Y and Si elements distributed homogeneously on Pr^{3+} -CTO photocatalysts (Fig. 4(e, f)), indicating the Pr^{3+} -YSO dispersed uniformly on the surface of Pr^{3+} -CTO to form large portions of Pr^{3+} -CTYS heterojunctions, through which the energy and carrier could be transferred effectively between them. Consequently, the UV light generated by Pr^{3+} -YSO could be used better by Pr^{3+} -CTO for overall splitting water.

Pt nanoparticles (NPs) mainly exist as metallic state (Fig. 5(c), Pt 4f XPS), and they exposed their high-energy (111) planes in Pr^{3+} -CTYS/Pt (Fig. 4(d)). The metallic Pt NPs are capable of promoting photogenerating hydrogen with lower the HER over-potential for Pr^{3+} -CTYS/Pt photo-catalysts. Paradoxically, photogenerated hydrogen and oxygen are prone to recombine on those metallic Pt NPs. As a result, the application of FDC oxygen transfer reagents is indispensable in our reactive system to capture and transfer newly generated O_2 for visible-light-driven overall splitting water.

4. Conclusion

In this work, a two-pronged strategy was designed to overcome two key obstacles for visible-light-driven overall water splitting by taking advantages of visible-to-ultraviolet UC effects as well as inhibiting rapid hydrogen-oxygen recombination over the photocatalyst. To fulfill that purpose, a photocatalyst was designed by assembling three components which included a visible-to-ultraviolet UC unit, a UV-responsive photocatalyst and an oxygen transfer reagent. As the first strategy, the visible-to-ultraviolet UC units on the photocatalyst was able to transfer incident visible irradiation to UV light emission. Owing to large area of heterojunction constructed between the Visible-to-ultraviolet UC unit

and UV-responsive photocatalyst, the UV light yielded from the Visible-to-ultraviolet UC units were utilized effectively by the UV-responsive photocatalyst for overall water splitting. As for second strategy, oxygen reagent transfer FDC was applied to capture and transport photogenerated oxygen away from the photocatalyst surface, thus preventing the newly generated hydrogen and oxygen from recombining. The two-pronged strategy could open a new window for researches in photocatalytic hydrogen from pure water, not only because of its convenience and high efficiency, but its favorable versatility for UV-responsive semiconductor photocatalysts to realize overall split water by visible light irradiation.

Notes

The authors declare no competing financial interest.

Acknowledgments

This work is supported by the NSF of China (21433007, 21673262), Natural Science Foundation of Jiangsu Province (BK20130095), and Postdoctoral Science Foundation of China (146819), respectively.

Appendix A. Supplementary data

Supplementary data associated with this article can be found, in the online version, at <http://dx.doi.org/10.1016/j.apcatb.2017.04.063>.

References

- [1] M.S. Dresselhaus, I.L. Thomas, *Nature* 414 (2001) 332–337.
- [2] R.D. Cortright, R.R. Davda, J.A. Dumesic, *Nature* 418 (2002) 964–967.
- [3] G. Lu, S. Zhang, G. Hou, F. Shi, T. Li, X. Yao, H. Liang, *J. Mol. Catal. (China)* 30 (2016) 383–390.
- [4] H. Gao, W. Zhen, J. Ma, G.X. Lu, *Appl. Catal. B* 206 (2017) 353–363.
- [5] M. Gratzel, *Acc. Chem. Res.* 14 (1981) 376–384.
- [6] Z. Li, B. Tian, W. Zhang, X. Zhang, Y. Wu, G.X. Lu, *Appl. Catal. B* 204 (2017) 33–42.
- [7] W. Wang, G.X. Lu, *Prog. Chem.* 15 (2003) 74–78.
- [8] G.X. Lu, S.B. Li, *Int. J. Hydrogen Energy* 17 (1992) 767–770.
- [9] G.X. Lu, H. Gao, J. Suo, S.B. Li, *J. Chem. Soc. Chem. Commun.* 21 (1994) 2423–2424.
- [10] X. Wang, S. Bai, Z. Bao, *J. Mol. Catal. (China)* 29 (2015) 266–274.
- [11] A. Fujishima, K. Honda, *Nature* 238 (1972) 37–38.
- [12] C. Wang, Q.Q. Hu, J.Q. Huang, L. Wu, Z.H. Deng, Z.G. Liu, Y. Liu, Y.G. Cao, *Appl. Surf. Sci.* 283 (2013) 188–192.
- [13] Z. Li, B. Tian, W. Zhen, Y. Wu, G. Lu, *Appl. Catal. B* 203 (2017) 408–415.
- [14] B. Tian, W. Zhen, H. Gao, X. Zhang, Z. Li, G.X. Lu, *Appl. Catal. B* 203 (2017) 789–797.
- [15] W. Zhen, F. Gao, B. Tian, P. Ding, Y. Deng, H. Gao, G.X. Lu, *J. Catal.* 348 (2017) 200–211.
- [16] X. Zhang, G.X. Lu, *Carbon* 108 (2016) 215–224.
- [17] X. Zhao, G.X. Lu, *Int. J. Hydrogen Energy* 41 (2016) 13993–14002.
- [18] W. Zhen, J. Ma, G.X. Lu, *Appl. Catal. B* 190 (2016) 12–25.
- [19] Z. Li, Y. Wu, G.X. Lu, *Appl. Catal. B* 188 (2016) 56–64.
- [20] W. Zhen, H. Gao, B. Tian, G.X. Lu, *ACS Appl. Mater. Interface* 8 (2016) 10808–10819.
- [21] Y. Guo, G.X. Lu, *Int. J. Hydrogen Energy* 41 (2016) 6706–6712.
- [22] B. Tian, Z. Li, W. Zhen, G.X. Lu, *J. Phys. Chem. C* 120 (2016) 6409–6415.
- [23] X. Zhao, G.X. Lu, *Int. J. Hydrogen Energy* 41 (2016) 3349–3362.
- [24] Z. Li, C. Kong, G.X. Lu, *J. Phys. Chem. C* 120 (2016) 56–63.
- [25] W. Zhang, G.X. Lu, *Catal. Sci. Technol.* 6 (2016) 7693–7697.
- [26] W. Zhang, C. Kong, W. Gao, G.X. Lu, *Chem. Commun.* 52 (2016) 3038–3041.
- [27] C. Kong, Z. Li, G.X. Lu, *Int. J. Hydrogen Energy* 40 (2015) 9634–9641.
- [28] Z. Li, C. Kong, G.X. Lu, *Int. J. Hydrogen Energy* 40 (2015) 9061–9068.
- [29] Z. Li, Q. Wang, C. Kong, G.X. Lu, *J. Phys. Chem. C* 119 (2015) 13561–13568.
- [30] C. Kong, Z. Li, G.X. Lu, *Int. J. Hydrogen Energy* 40 (2015) 5824–5830.
- [31] W. Zhen, B. Li, G.X. Lu, *Chem. Commun.* 51 (2015) 1728–1731.
- [32] C. Kong, S. Min, G.X. Lu, *Chem. Commun.* 50 (2014) 9281–9283.
- [33] E. Cui, G.X. Lu, *Int. J. Hydrogen Energy* 39 (2014) 7672–7685.
- [34] L. Li, Y. Huang, A. Zhang, M. Xiang, J. Yang, M. Jiao, *J. Mol. Catal. (China)* 30 (2016) 470–479.
- [35] C. Kong, S. Min, G.X. Lu, *ACS Catal.* 4 (2014) 2763–2769.
- [36] W.J. Jiang, L. Gu, L. Li, Y. Zhang, X. Zhang, L.J. Zhang, J.Q. Wang, J.S. Hu, Z.D. Wei, L.J. Wan, *J. Am. Chem. Soc.* 138 (2016) 3570–3578.

- [37] C. Kong, S. Min, G.X. Lu, *Int. J. Hydrogen Energy* 39 (2014) 4836–4844.
- [38] C. Kong, S. Min, G.X. Lu, *Chem. Commun.* 50 (2014) 5037–5039.
- [39] Y. Wu, G.X. Lu, *Phys. Chem. Chem. Phys.* 16 (2014) 4165–4175.
- [40] Y. Wu, G.X. Lu, S.B. Li, J. Photochem. Photobiol. A. Chem. 181 (2006) 263–267.
- [41] X. Zhang, Z. Jin, Y. Li, G.X. Lu, *J. Power Source* 166 (2007) 74–79.
- [42] T.K. Townsend, N.D. Browning, F.E. Osterloh, *ACS Nano* 6 (2012) 7420–7426.
- [43] C. Li, Z. Lei, Q. Wang, F. Can, F. Wang, W. Shangguan, *J. Mol. Catal. (China)* 29 (2015) 382–389.
- [44] Q. Zhang, J.P. Ge, T. Pham, J. Goebel, Y.X. Hu, Z.D. Lu, Y.D. Yin, *Angew. Chem. Int. Ed.* 48 (2009) 3516–3519.
- [45] M. Higashi, K. Domen, R. Abe, *Energy Environ. Sci.* 4 (2011) 4138–4147.
- [46] B. Li, W. Zhen, G. Lu, J. Ma, *J. Mol. Catal. (China)* 29 (2015) 152–163.
- [47] Q. Hu, J. Huang, G. Li, J. Chen, Z. Zhang, Z. Deng, Y. Jiang, W. Guo, Y. Cao, *Appl. Surf. Sci.* 369 (2016) 201–206.
- [48] E. Cui, G. Lu, *Int. J. Hydrogen Energy* 39 (2014) 8959–8968.
- [49] B. Qiu, Q. Zhu, M. Du, L. Fan, M. Xing, J. Zhang, *Angew. Chem.* 129 (2017) 2728–2732.
- [50] S. Hong, D.P. Kumar, D.A. Reddy, J. Choi, T.K. Kim, *Appl. Surf. Sci.* 396 (2017) 421–429.
- [51] A.P. Gaikwad, D. Tyagi, C.A. Betty, R. Sasikala, *Appl. Catal. A Gen.* 517 (2016) 91–99.
- [52] D.J. Martin, P.J.T. Reardon, S.J.A. Moniz, J. Tang, *J. Am. Chem. Soc.* 136 (2014) 12568–12571.
- [53] D. Ke, S. Liu, K. Dai, J. Zhou, L. Zhang, T. Peng, *J. Phys. Chem. C* 113 (2009) 16021–16026.
- [54] T. Mahvelati-Shamsabadi, E.K. Goharshadi, *Ultrason. Sonochem.* 34 (2017) 78–89.
- [55] S.K. Apte, S.N. Garaje, S.D. Naik, R.P. Waichal, J.O. Baeg, B.B. Kale, *Nanoscale* 6 (2014) 908–915.
- [56] H. Mizoguchi, K. Ueda, M. Orita, S.C. Moon, K. Kajihara, M. Hirano, H. Hosono, *Mater. Res. Bull.* 37 (2002) 2401–2406.
- [57] P.T. Diallo, K. Jeanlouis, P. Boutinaud, R. Mahiou, J.C. Cousseins, *J. Alloy Compd.* 323 (2001) 218–222.
- [58] K. Iwashina, A. Iwase, Y.H. Ng, A. Rose, A. Kudo, *J. Am. Chem. Soc.* 137 (2015) 604–607.
- [59] W. Zhu, X. Yue, W. Zhang, S. Yu, Y. Zhang, J. Wang, J. Wang, *Chem. Commun.* 52 (2016) 1486–1489.
- [60] J. Wang, H. Zhong, Z. Wang, F. Meng, X. Zhang, *ACS Nano* 10 (2016) 2342–2348.
- [61] K. Maeda, T. Takata, M. Hara, N. Saito, Y. Inoue, H. Kobayashi, K. Domen, *J. Am. Chem. Soc.* 127 (2005) 8286–8287.
- [62] R. Abe, M. Higashi, K. Domen, *J. Am. Chem. Soc.* 132 (2010) 11828–11829.
- [63] M. Higashi, K. Domen, R. Abe, *Energy Environ. Sci.* 4 (2011) 4138–4147.
- [64] H. Fujito, H. Kunioku, D. Kato, H. Suzuki, M. Higashi, H. Kageyama, R. Abe, *J. Am. Chem. Soc.* 138 (2016) 2082–2085.
- [65] D. Dontsova, C. Fettkenhauer, V. Papaefthimiou, J. Schmidt, M. Antonietti, *Chem. Mater.* 28 (2016) 772–778.
- [66] G. Zhang, Z.A. Lan, L. Lin, S. Lin, X. Wang, *Chem. Sci.* 7 (2016) 3062–3066.
- [67] D. Zheng, X.N. Cao, X. Wang, *Angew. Chem. Int. Ed.* 55 (2016) 11512–11516.
- [68] M. Jung, J.N. Hart, D. Boensch, J. Scott, Y.H. Ng, R. Amal, *Appl. Catal. A Gen.* 518 (2016) 221–230.
- [69] H. Lin, C. Shih, *Catal. Surv. Asia* 16 (2012) 231–239.
- [70] H. Lin, C. Shih, *J. Mol. Catal. A: Chem.* 411 (2016) 128–137.
- [71] E.L. Cates, S.L. Chinnapongse, J.H. Kim, J.H. Kim, *Environ. Sci. Technol.* 46 (2012) 12316–12328.
- [72] W.Y. Zhang, C. Kong, G.X. Lu, *Chem. Commun.* 51 (2015) 10158–10161.
- [73] E. Lalik, A. Drelinkiewicz, R. Kosydar, R. Tokarz-Sobieraj, M. Witko, T. Szumelda, J. Gurgul, D. Duraczyńska, *Appl. Catal. A: Gen.* 517 (2016) 196–210.
- [74] E. Lalik, A. Drelinkiewicz, R. Kosydar, R. Tokarz-Sobieraj, M. Witko, T. Szumelda, J. Gurgul, D. Duraczyńska, *Appl. Catal. A: Gen.* 517 (2016) 196–210.
- [75] S. Li, Y. Guo, L. Zhang, J. Wang, Y. Li, Y. Li, B. Wang, *J. Power Sources* 252 (2014) 21–27.
- [76] W. Qin, D. Zhang, D. Zhao, L. Wang, K. Zheng, *Chem. Commun.* 46 (2010) 2304–2306.
- [77] C. Hu, C. Sun, J. Li, Z. Li, H. Zhang, Z. Jiang, *Chem. Phys.* 325 (2006) 563–566.
- [78] E.L. Cates, A.P. Wilkinson, J.H. Kim, *J. Lumin.* 160 (2015) 202–209.
- [79] W. Zhang, S. Yang, J. Li, W. Gao, Y. Deng, W. Dong, *Appl. Catal. B: Environ.* 206 (2017) 89–103.
- [80] J.G. Riess, M. Le Blanc, *Angew. Chem. Int. Ed.* 17 (1978) 621–634.
- [81] Z.S. Khan, A. Ali, Z. Nazir, X. Cao, *J. Non-Cryst. Solids* 432 (2016) 540–544.
- [82] S.S. Arbuj, R.R. Hawaldar, S. Varma, S.B. Waghmode, B.N. Wani, *Sci. Adv. Mater.* 4 (2012) 568–572.